

**T.C.
BAHÇEŞEHİR UNIVERSITY**

**USE OF PARK TRANSFORMATION IN HARMONIC
SUPPRESSION FOR WAVELET PACKET BASED
BROKEN ROTOR BAR DETECTION**

M.S. Thesis

Ferzan GÜRAN

İstanbul, 2011

T.C.
BAHÇEŞEHİR UNIVERSITY
The Graduate School of Natural and Applied Sciences
Electrical and Electronics Engineering

**USE OF PARK TRANSFORMATION IN HARMONIC
SUPPRESSION FOR WAVELET PACKET BASED
BROKEN ROTOR BAR DETECTION**

M.S. Thesis

Ferzan GÜRAN

Supervisor: Dr. Levent EREN

İstanbul, 2011

T.C
BAHÇEŞEHİR ÜNİVERSİTESİ
The Graduate School of Natural and Applied Sciences
Electrical and Electronics Engineering

Title of the Master's Thesis : Use of Park Transformation in Harmonic Suppression
for Wavelet Packet Based Broken Rotor Bar Detection
Name/Last Name of the Student : Ferzan GÜRAN
Date of Thesis Defense : 09.09.2011

The thesis has been approved by the Graduate School of Natural and Applied Sciences.

Assoc. Prof. F. Tunç BOZBURA
Acting Director

This is to certify that we have read this thesis and that we find it fully adequate in scope, quality and content, as a thesis for the degree of Master of Science.

Examining Committee Members:

Asst. Prof. Dr. Levent EREN (Supervisor) :

Prof. Dr. Emin TACER :

Asst. Prof. Dr. Yalçın ÇEKİÇ :

ACKNOWLEDGEMENT

I want to state that without the precious helps of Dr. Levent EREN, this thesis would not come to true. His guidance and extensive knowledge on the topic, clarified the questions and difficulties came about during the study.

I thank the other members of my committee, Dr. Emin TACER and Dr. Yalçın ÇEKİÇ for getting in to my presentation.

I also thank to Development and City Planning principle of Çekmeköy Municipality Dr. Eyüp Salih ELMAS for his tolerance during work hours.

At last, I appreciate my wife Ayşe GÜRAN being so kind, understandable and encouraging during my study though she has to deal with another member of the family little Halid Ziya, our son.

ABSTRACT

USE OF PARK TRANSFORMATION IN HARMONIC SUPPRESSION FOR WAVELET PACKET BASED BROKEN ROTOR BAR DETECTION

Güran, Ferzan

Electrical and Electronics Engineering
Supervisor: Asst. Prof. Dr. Levent EREN

September 2011, 45 pages

Electric motors are the most important equipments of modern industrial production and services. Naturally, any problem concerning these electric machines decreases the efficiency of production and cause major losses in these facilities. Most of these failures occur as bearing, stator winding and broken rotor bar faults. Those faults can be recognized from the data gathered from the motor current signatures.

General methods are based on using a notch filter for suppressing power system harmonics and then analyse the current signatures by the fourier analyse procedure. Working with time domain information or frequency domain information does not give the expected results.

We in this study, used Park's transformation for suppressing fundamental power system harmonic and wavelet packets to analyse the stator currents in order to identify broken rotor bar failures in an induction motor. In order to verify that the increase in the energy levels of fault associated frequency bands are indeed due to the broken rotor bars, spectral post processing with fast fourier transform is applied.

Keywords: Induction Motors, Park's Transformation, Fourier Analysis, Wavelets, Wavelet Packets.

ÖZET

DALGACIK PAKETİ KULLANILARAK KIRIK ROTOR ÇUBUĞU TESPİTİNDE HARMONİK BASTIRIMI İÇİN PARK DÖNÜŞÜMÜNÜN KULLANILMASI

Güran, Ferzan

Elektrik ve Elektronik Mühendisliği
Danışman: Yrd. Doç. Dr. Levent EREN

Eylül 2011, 45 sayfa

Elektrik motorları, modern endüstriyel üretim için en mühim ekipmanlardır. Bu ekipmanlarda meydana gelen herhangi bir aksaklık, üretim veriminin düşmesine ve işletmelerde büyük kayıplara yol açmaktadır. Problemler sıklıkla rulmanlarda, stator sargılarında ve rotor çubuklarında görülür. Meydana gelen hatalar, motor akım işaretlerinden toplanan verilerle tanımlanabilir.

Geleneksel olarak analizler, güç sistem harmoniklerinin band durduran filtrelerle elimine edilmesinden sonra akım işaretlerinin fourier dekompozisyonu ile gerçekleştirilir. Sadece zaman veya frekans domeninde analiz beklenen sonuçları vermemektedir.

Bu çalışmada, motorun statorundan aldığımız akım işaretlerini güç sistem harmoniğini bastırmak için park dönüşümüne tabi tuttuk. Bu dönüşümden elde edilen akım bileşenleri arızayı tespit için dalgacık paketleri ile analiz edildi. İlgili frekans bantları için enerji seviyelerinin tespiti yapılmış olup, bantlardaki enerji seviyelerinin kırık rotor çubuklarından kaynaklandığını doğrulamak üzere hızlı fourier dönüşümü ilgili bantlara uygulanmıştır.

Anahtar Kelimeler: Asenkron Motorlar, Park Dönüşümü, Fourier Analizi, Dalgacıklar, Dalgacık Paketleri.

TABLE OF CONTENTS

ACKNOWLEDGEMENT	iii
ABSTRACT	iv
ÖZET	v
TABLE OF CONTENTS	vi
LIST OF ABBREVIATIONS	vii
LIST OF SYMBOLS	viii
LIST OF FIGURES	ix
1. INTRODUCTION.....	1
2. LITERATURE REVIEW	3
3. MOTOR FAULTS AND DETECTION METHODS	4
3.1 MOTOR FAULTS	4
3.2 MOTOR CURRENT SIGNATURE ANALYSIS	4
4. FAULT DETECTION METHOD	6
4.1 SIGNAL ANALYSIS	6
4.1.1 Fourier Transform.....	6
4.1.2 Discrete Time Fourier Transform.....	7
4.1.3 Short Time Fourier Transform	7
4.1.4 Wavelets	8
4.1.5 Wavelet Transforms	9
4.3 PARK'S TRANSFORMATION	16
5. ASSESSING OF THE ALGORITHM AND TESTING WITH REAL DATA	21
5.1 TEST SETUP	21
5.2 TEST PROCEDURE	23
5.3 TESTING OF THE ALGORITHM USING SIMULATED DATA	24
5.4 TESTING WITH HEALTHY MOTOR DATA	29
5.5 TESTING WITH FAULTY MOTOR DATA	32
6. CONCLUSION AND FUTURE WORK.....	36
REFERENCES	37
APPENDIX	41
CURRICULUM VITAE	45

LIST OF ABBREVIATIONS

Analog To Digital Conversion	:	A/D
Continuous Wavelet Transform	:	CWT
Daubechies 10 Wavelet	:	DB
Discrete Time Fourier Transform	:	DTFT
Discrete Wavelet Transform	:	DWT
Fast Fourier Transform	:	FFT
High Pass Filter	:	HPF
Infinite Impulse Response	:	IIR
Low Pass Filter	:	LPF
Lower Sideband Magnitude	:	A_L
Motor Current Signature Analysis	:	MCSA
Root Mean Square	:	RMS
Short Time Fourier Transform	:	STFT
Upper Sideband Magnitude	:	A_R
Wavelet Transform	:	WT

LIST OF SYMBOLS

Angular Frequency	:	ω
Broken Rotor Bar Frequency	:	f_b
Magnetizing Current	:	i_d
Mother Wavelet	:	ψ
Per Unit Slip	:	s
Supply Frequency	:	f_e
Torque Producing Current	:	i_q

LIST OF FIGURES

Figure 4.1: A db10 wavelet and a sine wave	8
Figure 4.2: Wavelets of different scales and positions	10
Figure 4.3: (a) Two band analysis filter bank. (b) Downsampling by two	12
Figure 4.4: Wavelet decomposition tree (three levels).....	12
Figure 4.5: One-stage DWT with high-frequency noise added.	13
Figure 4.6: The frequency responses of analysis filter bank in WT case	13
Figure 4.7: Binary tree.....	14
Figure 4.8: Constant bandwidth separation.....	14
Figure 4.9: Direct and Quadrature axis components	16
Figure 5.1: Test setup for induction motor with a single broken rotor bar	22
Figure 5.2: Flow chart Diagram	24
Figure 5.3: Both healthy rotor bars and two broken bars with Fourier transform	25
Figure 5.4: Simulated phase current	26
Figure 5.5: Direct current component from Park's transformation.....	27
Figure 5.6: Wavelet Packet Coefficients 0-7.5 Hz. Band	28
Figure 5.7: FFT of the direct component	29
Figure 5.8: Healthy case phase current	30
Figure 5.9: Direct current component.....	31
Figure 5.10: Wavelet Packet Coefficients 0-7.5 Hz. Band	31
Figure 5.11: FFT of the direct component	32
Figure 5.12: Faulty case phase current	33
Figure 5.13: Direct current component.....	34
Figure 5.14: Wavelet Packet Coefficients 0-7,5 Hz. Band	34
Figure 5.15: FFT of the direct component	35

1. INTRODUCTION

In today's industrial applications, induction motors are used widely. As they are used heavily, they fail due to faults like bearing damage, insulation damage, broken rotor bars or over loading and so on. Heavy reliance of modern industry on these machines, enforces the need for monitoring the condition of these machines in order to avoid the unpredictable shutdowns.

Bearing faults, insulation faults, and rotor faults are the primary causes of motor failures accounting for about a percentage of 50, 35, and 10 all induction motor failures respectively (Kliman 1997). Resulting as a number of problems, effective techniques are to be improved to detect, analyze and prevent electrical machine failures. One of these methods for detecting faults in electrical equipment is Motor Current Signature Analysis (MCSA), developed by scientists at Oak Ridge National Laboratory providing nonintrusive means for detecting the mechanical and electrical problems in both motor and driven equipment (Kryter and Haynes 1989).

Signal processing operations such as Fourier and wavelet transforms help us determine the magnitude of the fault related frequencies. The changes in the amplitudes of fault frequencies indicate the state of the defect.

Since the fundamental component amplitude is extremely high compared to the other components, smaller but important signals will be difficult to detect. This way, changes in the amplitude of some components related to the failure may be unnoticed. Usually, the fundamental component is suppressed by filtering the current signal in preprocessing.

Analog filters are sensitive to temperature variations, which may shift the filter resonance frequency and degrade the desired response (Bonaldi, et al. 2003). Therefore, the use of digital filters is preferred. Generally, notch filters are used to remove the fundamental component.

The subject of this study is detecting the broken rotor bar fault of an induction motor, using wavelet packet decomposition of motor current data. The current data is

preprocessed by Park's Transformation to remove the fundamental component as the amplitude of the fundamental frequency is greater than the sideband amplitude. In the proposed method, there is no need for a notch filter, therefore, the proposed approach provides lower computational complexity. Furthermore, the transform will demodulate the fault frequency and provide better separation of signature frequency from the fundamental frequency.

In the proposed method, three phase currents are going to be transformed to direct and quadrature components using Park's transform algorithm. The signature frequency components are demodulated in magnetizing (i_d) and torque producing current (i_q) obtained by the transform. The direct current component will be decomposed into equally spaced frequency bands by using all-pass implementation of elliptic IIR half-band filter. Next, energy level of each frequency band is going to be calculated by determining rms values from WPCs of associated frequency bands. The changes in the energy levels of frequency bands in which broken rotor bar related current frequencies lie are monitored to detect motor fault condition.

In order to verify that the increase in the energy levels of fault associated frequency bands are indeed due to the broken rotor bars, spectral post processing will be applied. Fast Fourier transform of the 0-7.5 Hz. band will be calculated. This will be the verification for both simulated and real data showing that the proposed approach is effective in detecting broken rotor bars. In all analysis, Matlab is used for its simplicity, high performance calculation ability and powerful visual data analyzing tools.

Literature review will be presented in chapter two. Information about motor faults and motor current signature analysis is provided in chapter three. Signal processing methods including Fourier and wavelet transforms, broken bar detection procedure are cited in chapter four. Also dq0 transform, commonly known as Park's transformation, which composes the most important part of our contribution to the subject is featured. In the following chapter test setup, results of simulated and test data are presented. The last chapter will be the conclusion part.

2. LITERATURE REVIEW

Various methods are developed in signal processing. One of these methods is wavelet analysis, evolved in early 1900's by Alfred Haar. The application of this method to seismic signals starts with J. Morlet in 1982. Ingrid Daubechies, opened the door for a new system of image compression that allows for the efficient storage of an image without sacrificing detail.

Generally, Fourier transforms have been used in motor current signature analysis. By using the Fourier transform, fault signatures can be detected but time location is lost due to the lack of algorithm. Valens, described the superiorities of wavelets over Fourier analysis on mathematical and engineering aspects.

Wavelets found a specific application area in electrical engineering because of its multi resolution analysis characteristic. Eren and Devaney (2001), analyzed the starting current transient of an induction motor is analyzed via discrete wavelet transform to detect bearing faults. The frequency subbands for bearing pre-fault and post-fault conditions were compared to identify the effects of bearing/machine resonant frequencies as the motor starts. Arslan, Orhan and Aktürk (2003), stated that data gathered from the motor can be used in fault analysis. Şeker and Ayaz (2003), extracted features from vibration signals measured from motors subjected to accelerated bearing fluting aging and detected the effects of bearing fluting at each aging cycle of induction motors. Eren, Devaney and Çekiç (2003), studied on the detection of broken rotor bar in an induction machine via wavelet packet decomposition.

Bonaldi et al. (2003), by extracting the supply component frequency found that it is possible to improve the dynamic range of the A/D converter in order to get a more precise digitized signal and improve the failure detection. Cusido et al. (2006), analyzed the current spectra of dq0 Park components with MCSA method and claimed to improve earlier fault detection by using wavelet transform as signal analysis method and found it to be possible for reducing signal noise effects.

3. MOTOR FAULTS AND DETECTION METHODS

3.1 MOTOR FAULTS

Bearing and broken rotor bar faults are mechanical faults that occur motor failures. Insulation, rotor, stator winding and bearing faults are the most common problems resulting the motor failures. Major faults of electrical machines can broadly be classified as follows:

- Stator faults resulting in the opening or shorting of one or more of a stator phase windings.
- Abnormal connection of the stator windings
- Broken rotor bar or cracked rotor end-rings
- Static and/or dynamic air-gap irregularities
- Bent shaft which can result in a rub between the rotor and stator, causing serious damage to stator core and windings.

Motor Current Signature Analysis (MCSA) is the best possible option for its non-intrusive approach and also uses the stator winding as the search coil (Mehla and Dahiya, 2007).

3.2 MOTOR CURRENT SIGNATURE ANALYSIS

Motor Current Signature Analysis (MCSA) is an electric machinery monitoring technology developed by the Oak Ridge National Laboratory. It provides a highly sensitive, selective, and cost-effective means for on-line line monitoring of a wide variety of heavy industrial machinery. Extensive test data support that MCSA has a number of inherent strengths, the most notable being that it:

- Provides nonintrusive monitoring away from the equipment,
- Provides degradation and diagnostic information comparable to conventional instrumentation,

- Offers high sensitivity to a variety of mechanical disorders affecting operational readiness,
- Offers means for separating one form of disorder from another,
- Can be used by relatively unskilled personnel.
- Can be applied to high-powered and fractional horsepower machines, ac and dc motors (Pillay and Xu).

A motor current signal is ideally a sinusoidal wave. We can represent the current either in terms of time or frequency. The amplitude of the peak in frequency is equal to the RMS amplitude of the sine wave. Conversion of the current from time to frequency domain is achieved using the Fast Fourier Transform (FFT).

During actual operation, many harmonics will be seen in the motor signal, so that signal will show many peaks including line frequency and harmonics. This is known as the motor's current signature. Analyzing these harmonics after amplification and signal conditioning will enable identification of the various motor faults. Certain harmonics come in on the supply and these are of little consequence. However harmonics are also generated due to various electrical and mechanical faults. All faults cause a change in the internal flux distribution, generating the harmonics. These are intermediate harmonics and can not be detected by standard harmonic analyzers. As fault generated harmonics appear only in the current spectrum but not in voltage, superimposition of current and voltage spectra can easily identify them.

4. FAULT DETECTION METHOD

4.1 SIGNAL ANALYSIS

A signal has two components, amplitude and frequency. Frequency and amplitude data can be identified in a constant plane, time domain. In signal analysis, defining a signal in the time domain forms the basic operations of signal analysis.

The frequency and amplitude data of signals can be achieved by doing some mathematical operations. Signals encountered in real life applications are usually continuous time. To facilitate digital processing, a continuous time signal must be converted to a sequence of numbers. This process is known as sampling. After sampling signal can be analyzed in an electronic environment using mathematical operations. Extensive mathematical technique used for this analyze is the Fourier transform.

4.1.1 Fourier Transform

Fourier series clearly opens the frequency domain as an interesting and useful way of determining how circuits and systems respond to periodic input signals. Addressing these issues requires us to find the Fourier spectrum of all signals, both periodic and nonperiodic ones. We need a definition for the Fourier spectrum of a signal, periodic or not. This spectrum is calculated by what is known as the Fourier Transform.

Mathematically, the process of Fourier analysis is represented by the Fourier transform:

$$F(\omega) = \int_{-\infty}^{\infty} f(t) e^{-j\omega t} dt \quad (4.1)$$

which is the sum over all time of the signal $f(t)$ multiplied by a complex exponential. The results of the transform are the Fourier coefficients, which when $F(\omega)$ multiplied by a sinusoid of appropriate frequency, yield the constituent sinusoidal components of the original signal.

The information provided by the integral, corresponds to all time values, since the integration is from minus to plus infinity over time. Whether the frequency component appears at time t_1 or t_2 it will have the same effect on the integration. This reminds us that Fourier transform is not suitable if the signal has time varying frequency, i.e., the signal is non-stationary (Polikar, 1994).

4.1.2 Discrete Time Fourier Transform

The Discrete Time Fourier Transform (DTFT) is a Fourier transform that operates on a periodic, discrete signals. If we imagine that we acquire an n sample signal, and want to find its frequency spectrum by using the DFT, the signal can be decomposed into sine and cosine waves with frequencies equally spaced between zero and one-half of the sampling rate. As mentioned before, padding the time domain signal with zeros makes the period of the time domain longer, as well as making the spacing between samples in the frequency domain narrower. As n approaches infinity, the time domain becomes a periodic, and the frequency domain becomes a continuous signal. This is the DTFT, the Fourier transform that relates an aperiodic, discrete signal, with a periodic, continuous frequency spectrum (Smith, 2003).

4.1.3 Short Time Fourier Transform

In an effort to correct this deficiency, Dennis Gabor (1946) adapted the Fourier transform to analyze only a small section of the signal at a time a technique called windowing the signal. Gabor's adaptation, called the Short-Time Fourier Transform (STFT), maps a signal into a two-dimensional function of time and frequency.

$$\text{STFT}(\tau, \omega) = \int_{-\infty}^{+\infty} f(x)w(t - \tau)e^{-i\omega t} dt \quad (4.2)$$

While the STFT's compromise between time and frequency information can be useful, the drawback is that once we choose a particular size for the time window, that window is the same for all frequencies. Many signals require a more flexible approach where we

can vary the window size to determine more accurately either time or frequency (Misiti et al. 2006).

4.1.4 Wavelets

The fundamental idea behind wavelets is to analyze according to scale. Indeed, some researchers in the wavelet field feel that, by using wavelets, one is adopting a whole new mindset or perspective in processing data.

Wavelets are mathematical functions that divide data into different frequency components, and then analyze each component with a resolution according to its scale. Their advantage over traditional Fourier method is; they can match physical situations where the signal contains discontinuities and sharp spikes. Wavelets were developed independently in the fields of mathematics, quantum physics, electrical engineering, and seismic geology. Interdisciplinary studies between these fields have led to many new wavelet applications such as image compression, turbulence, human vision, radar, and earthquake prediction (Graps, 1995).

A wavelet is a waveform of effectively limited duration that has an average value of zero. Compare wavelets with sine waves which are the basis of Fourier analysis, sinusoids do not have limited duration they extend from minus to plus infinity. And where sinusoids are smooth and predictable, wavelets tend to be irregular and asymmetric.

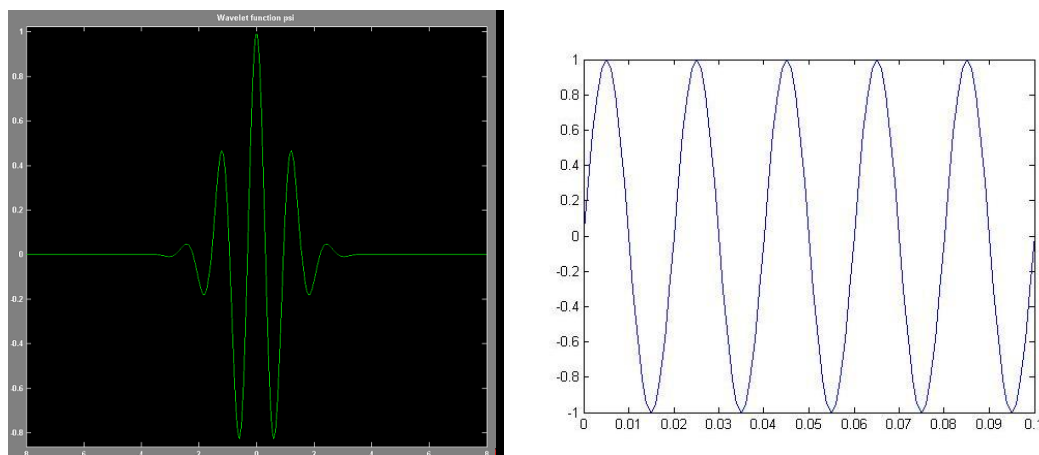


Figure 4.1: A db10 wavelet and a sine wave

Fourier analysis consists of breaking up a signal into sine waves of various frequencies. Similarly, wavelet analysis is the breaking up of a signal into shifted and scaled versions of the original (or mother) wavelet.

Just looking at picture of a wavelets and a sine wave, we can see intuitively that signals with sharp changes might be better analyzed with an irregular wavelet than with a smooth sinusoid. It also makes sense that local features can be described better with wavelets that have local extent.(Misiti et al. 2006)

4.1.5 Wavelet Transforms

Wavelet Transform is a transform which localizes a function both in space and scaling and has some desirable properties compared to the Fourier transform. The difference between the two transform is, Fourier transform decomposes the signal into sines and cosines, in contrary the wavelet transform uses functions that are localized in both the real and Fourier space (<http://gwyddion.net> 2011).

The wavelet transform or wavelet analysis is probably the most recent solution to overcome the shortcomings of the Fourier transform. In wavelet analysis the scalable window solves the signal-cutting problem. The window is shifted along the signal and the spectrum is calculated for every position. Then this process is repeated with scaling the window to a different value. The result will be the data of time-frequency representations of the signal, all with different resolutions. Because of this collection of representations we can speak of a multiresolution analysis. We can think the large scale as the big picture, while the small scales represent the zoomed situation. Wavelet transforms are broadly divided into three types: Continuous, Discrete and Multiresolution-based.

The continuous wavelet transform (CWT); is defined as the sum over all time of the signal multiplied by scaled, shifted versions of the wavelet function ψ :

$$\text{CWT (scale, position)} = \int_{-\infty}^{\infty} f(t)\psi(\text{scale, position, time})dt \quad (4.3)$$

- $\psi_{(s,a)}(t) = \frac{1}{\sqrt{s}}\psi\left(\frac{t-a}{s}\right)$
- $\psi = \text{Mother wavelet}$
- $s = \text{Scale}$
- $a = \text{Translation (shifting in time)}$
- $f = \text{Function to be analysed}$

The results of the CWT are wavelet coefficients C, which are a function of scale and position. Multiplying each coefficient by the appropriately scaled and shifted wavelet yields the constituent wavelets of the original signal.

Wavelet analysis produces a time-scale view of a signal. Scaling a wavelet simply means stretching (or compressing) it. The scale factor works exactly the same with wavelets. The smaller the scale factor, the more “compressed” the wavelet. Shifting a wavelet simply means delaying (or hastening) its onset. Mathematically, delaying a function $f(t)$ by k is represented by $f(t-k)$.

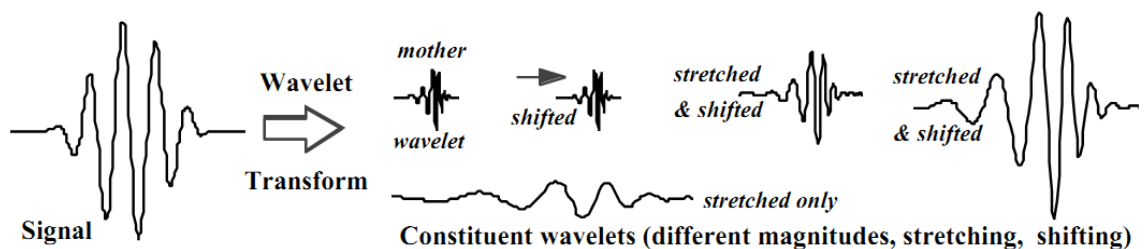


Figure 4.2: Wavelets of different scales and positions

Source: D. Lee Fugal, *Conceptual Wavelets In Digital Signal Processing*

The continuous wavelet transform is the sum over all time of the signal multiplied by scaled, shifted versions of the wavelet. This process produces wavelet coefficients that are a function of scale and position.

The discrete wavelet transform (DWT); is considerably easier to implement when compared to the CWT. Calculation of wavelet coefficients for every possible scale includes unnecessary information in to the signal. This causes the increase of the time taken for the calculation (Rioul, O., Vetterli). If the chosen scales and positions are taken at powers of two, analysis will be faster and more effective.

$$W(s,a)=\frac{1}{\sqrt{s}} \int f(t)\psi\left(\frac{t-a}{s}\right) dt \quad (4.4)$$

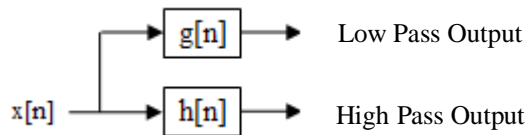
where $a = 2^j, b = k2^j$ and $j,k \in Z^2$

$$y_{Low}[k] = \sum_{n=-\infty}^{\infty} x[n]g[2k - n] \quad (4.5)$$

$$y_{High}[k] = \sum_{n=-\infty}^{\infty} x[n]h[2k - n] \quad (4.6)$$

$g[n]$, $h[n]$ and $y_x[k]$, are low pass and high pass filters and outputs respectively.

One filter of the analysis (wavelet transform) pair is a lowpass filter (LPF), while the other is a highpass filter (HPF). Each filter has a down-sampler after it, to make the transform efficient. A lowpass filter produces the average signal, while a highpass filter produces the detail signal. The low-frequency content gives the signal its identity. The high-frequency content represents the nuance. In wavelet analysis, words approximations and details are mentioned often. The approximations are the high-scale, low-frequency components of the signal. The details are the low-scale, high-frequency components.



(a)



(b)

Figure 4.3: (a) Two band analysis filter bank. (b) Downsampling by two

The original signal, passes through two complementary filters; low pass and high pass. If this operation is performed on a real digital signal, we come along with twice as much data as we started with. There exists a better and costless way to perform the decomposition using wavelets. One point out of two may be kept in each of the two samples to get the complete information. If decomposition is repeated, it is called the wavelet decomposition tree.

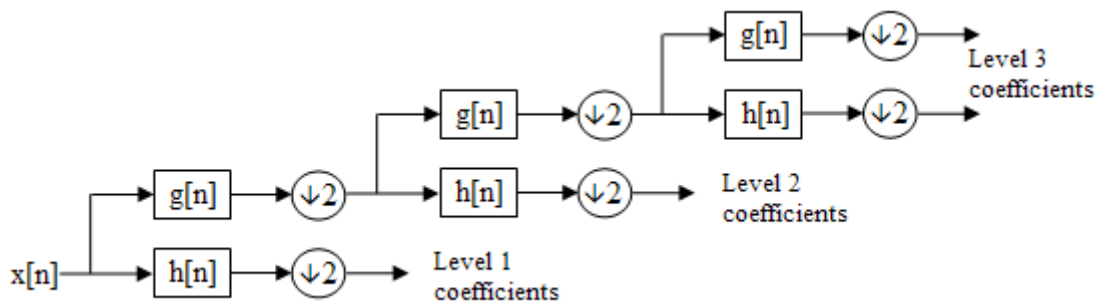


Figure 4.4: Wavelet decomposition tree (three levels).

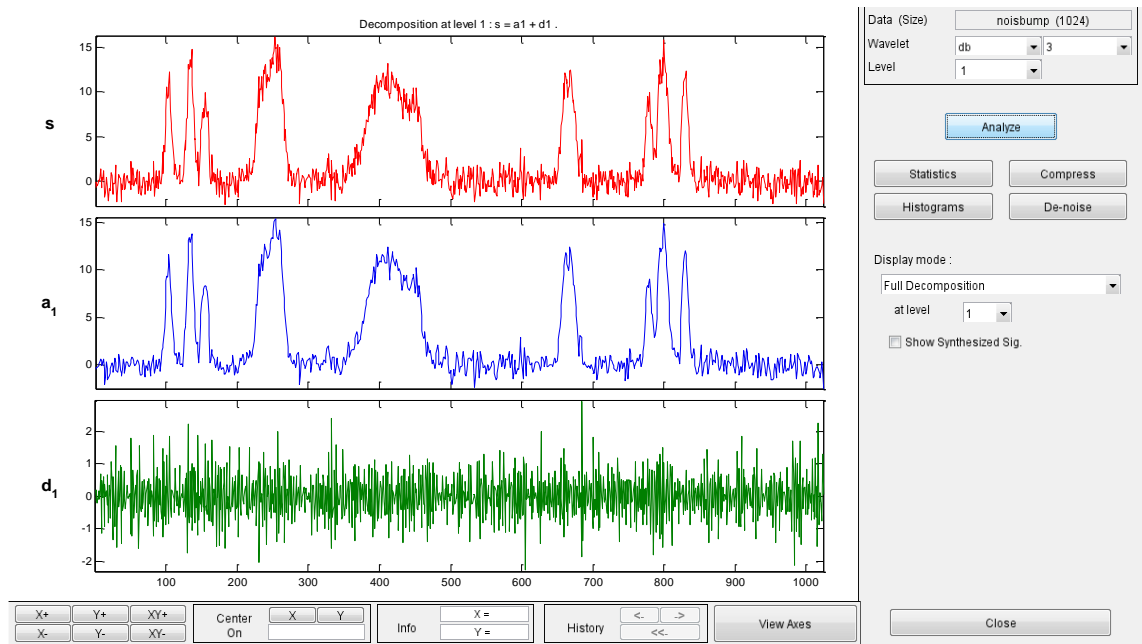


Figure 4.5: One-stage DWT with high-frequency noise added.

In the wavelet transform, the frequency responses of the analysis filter bank are spaced logarithmically.

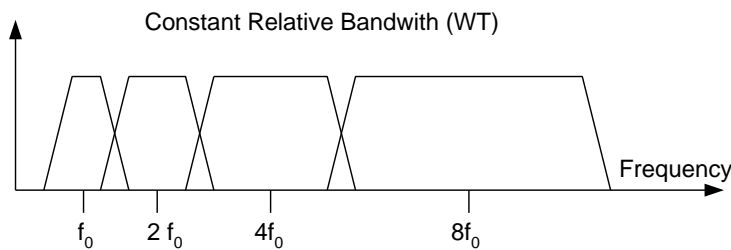


Figure 4.6: The frequency responses of analysis filter bank in WT case

Wavelet Packet Decomposition method is a generalization of wavelet decomposition that offers a richer range of possibilities for signal analysis. In wavelet analysis, a signal is split into an approximation and a detail. Filtering and gathering wavelet coefficients goes from the output of low frequency filter only. In wavelet packet analysis, the details can also be split as well as approximations. This yields more than 2^{2n-1} different ways to encode the signal. This forms the wavelet packet decomposition tree.

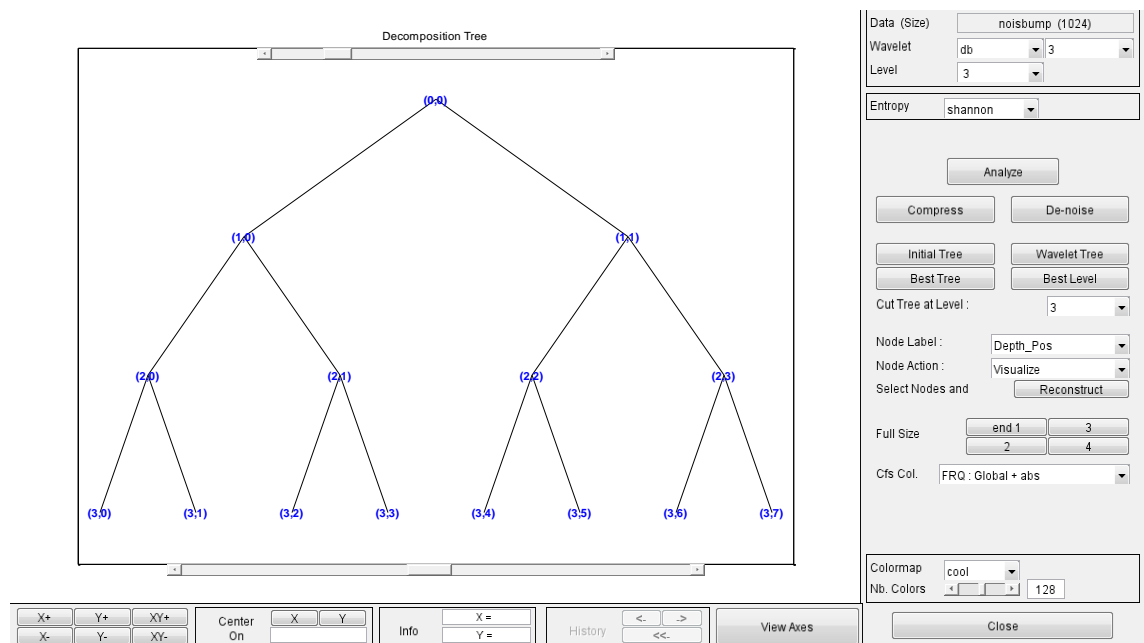


Figure 4.7: Binary tree

Wavelet packet decomposition has a constant frequency separation.

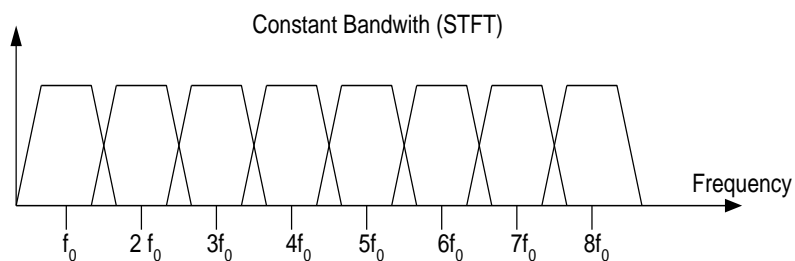


Figure 4.8: Constant bandwidth separation

4.2 Cracked or Broken Rotor Bar Detection

Cracked or broken rotor bars account for about 10% of motor failures. If a broken rotor bar exists, no current will flow in the rotor bar. The cracked or broken rotor bars can be detected from the current spectrum by determining the magnitude of the frequency components caused by this type of fault. The frequencies that are present in air gap flux, f_k , can be determined by the following equation (Kliman et al. 1988).

$$f_k = f_e \left[\frac{k}{p} (1-s) \pm s \right] \quad (4.7)$$

k = Harmonic index ($k= 1,2,3,\dots$)

s = Per unit slip

p = Number of fundamental pole pairs

f_e = Supply frequency

Due to the structure of a normal winding, the current spectrum will contain harmonics as given in above equation for: $k/p=1,5,7,11$, etc. Then, the broken rotor bar frequencies f_{rb} , for $k/p=1$ can be determined by the following equation (Eren, Çekiç and Devaney 2009).

$$f_b = f_e (1 \pm 2ks), k=1,2,3 \dots \quad (4.8)$$

where f_b represents the fault signature frequencies of the broken rotor bar.

A well-known effect of a broken bar is the appearance of the so-called sideband components (Toliat, Nand and Li (2005), Kliman et al. (2001), Benbouzid (2000)). These sidebands are found in the power spectrum of the stator current on the left and right sides of the fundamental frequency component. The lower side band component is caused by electrical and magnetic asymmetries in the rotor cage of an induction motor (Kliman et al. 2001), while the right sideband component is due to consequent speed ripples generated by the resulting torque pulsations.

Generally, the frequencies of the sideband components are very close to the frequency of the fundamental component, but the magnitudes of the sideband components are in the range of -20 to -60 dB, which are considerably smaller than the magnitude of the fundamental component. It is considered the fact that the amplitude of the fundamental frequency is extremely high if compared to the other signature components. So, smaller but more important signature components will get buried in the fundamental component. If the fundamental component has not been removed or filtered, changes in the amplitude of some signature components related to a fault may not be noticed while the fault is getting worse. Therefore, to solve this problem analog notch filters are used to remove the fundamental component (Benbouzid (2000), Thomson and Fenger

(2001), Benbouzid et al. (1999)). We, in this study use Park's transformation to remove the fundamental harmonic.

4.3 PARK'S TRANSFORMATION

This transformation is commonly used in three-phase electric machine models, where it is known as a Park transformation. It allows us to eliminate time-varying inductances by referring the stator and rotor quantities to a fixed or rotating reference frame (Krause, Wasynczuk, Sudhoff 1995). The transformation itself, known as the dq0 transformation, can be represented in a straightforward fashion in terms of the electrical angle θ (equal to poles/2 times the spatial angle θ) between the rotor direct axis and the stator phase-a axis (Fitzgerald, Kingsley and Umans 2003).

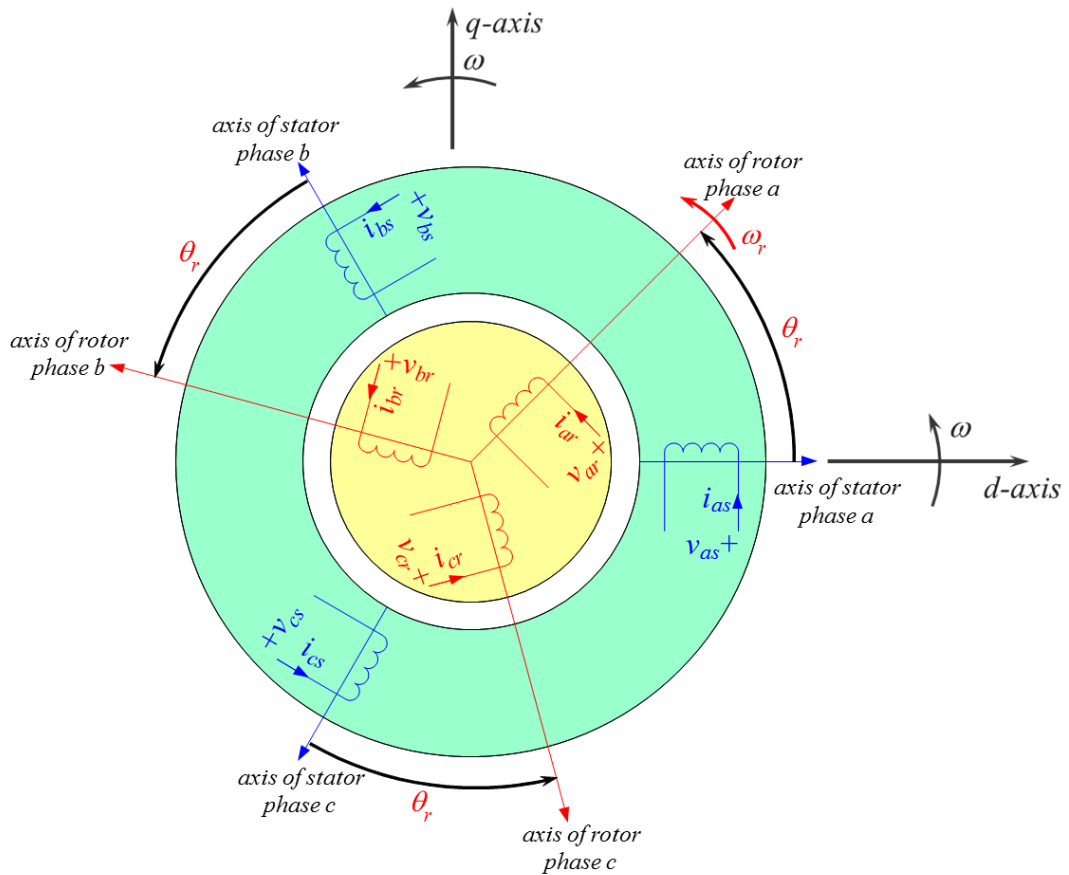


Figure 4.9: Direct and Quadrature axis components

S; stator quantity to be the transformed (current, voltage, or flux), $\theta = \omega t$ where θ is the angle between the rotor direct axis and stator phase a axis, we can write the transformation in matrix form as:

$$\begin{matrix} Sd \\ Sq \\ S0 \end{matrix} = \frac{2}{3} \begin{bmatrix} \cos\theta & \cos(\theta - 120) & \cos(\theta + 120) \\ \sin(\theta) & \sin(\theta - 120) & \sin(\theta + 120) \\ \frac{1}{2} & \frac{1}{2} & \frac{1}{2} \end{bmatrix} \begin{matrix} Sa \\ Sb \\ Sc \end{matrix} \quad (4.9)$$

and the inverse transformation as:

$$\begin{matrix} Sa \\ Sb \\ Sc \end{matrix} = \begin{bmatrix} \cos(\theta) & \sin(\theta) & 1 \\ \cos(\theta - 120) & \sin(\theta - 120) & 1 \\ \cos(\theta + 120) & \sin(\theta + 120) & 1 \end{bmatrix} \begin{matrix} Sd \\ Sq \\ S0 \end{matrix} \quad (4.10)$$

A third component, the zero-sequence component, is required to yield a unique transformation of the three stator-phase quantities; it corresponds to components of armature current which produce no net air- gap flux and hence no net flux linking the rotor circuits. As can be seen from equation (3.5), in a balanced condition, zero-sequence component does not exist. According to equation (3.5), dq0 components can be expressed as:

$$i_d = \frac{2}{3} [i_a \cos(2\pi f_e t) + i_b \cos(2\pi f_e t - 2\pi/3) + i_c \cos(2\pi f_e t + 2\pi/3)] \quad (4.11)$$

$$i_q = \frac{2}{3} [i_a \sin(2\pi f_e t) + i_b \sin(2\pi f_e t - 2\pi/3) + i_c \sin(2\pi f_e t + 2\pi/3)] \quad (4.12)$$

$$i_0 = 0 \quad (4.13)$$

where i_d and i_q represent direct axis and quadrature axis currents. The phase currents with a rotor fault can be modelled as below;

$$i_a = A \cos(2\pi f_e t) + A_L \cos(2\pi f_e t - 2\pi f_b t) + A_R \cos(2\pi f_e t + 2\pi f_b t) \quad (4.14)$$

$$i_b = A \cos(2\pi f_e t - 2\pi/3) + A_L \cos(2\pi f_e t - 2\pi f_b t - 2\pi/3) \quad (4.15)$$

$$+ A_R \cos(2\pi f_e t + 2\pi f_b t - 2\pi/3)$$

$$i_c = A \cos(2\pi f_e t + 2\pi/3) + A_L \cos(2\pi f_e t - 2\pi f_b t + 2\pi/3) \quad (4.16)$$

$$+ A_R \cos(2\pi f_e t + 2\pi f_b t + 2\pi/3)$$

where A_L , A_R , f_e and f_b are the lower side band magnitude, upper side band magnitude supply frequency and fault frequency of the broken rotor bar respectively.

We get the expressions below by replacing (4.14), (4.15) and (4.16) as appropriate with i_a , i_b and i_c in the equations (4.11) and (4.12).

$$i_d = \frac{2}{3} [[A \cos(2\pi f_e t) + A_L \cos(2\pi f_e t - 2\pi f_b t) + A_R \cos(2\pi f_e t + 2\pi f_b t)] \cos(2\pi f_e t) + [A \cos(2\pi f_e t - 2\pi/3) + A_L \cos(2\pi f_e t - 2\pi f_b t - 2\pi/3) + A_R \cos(2\pi f_e t + 2\pi f_b t - 2\pi/3)] \cos(2\pi f_e t - 2\pi/3) + [A \cos(2\pi f_e t + 2\pi/3) + A_L \cos(2\pi f_e t - 2\pi f_b t + 2\pi/3) + A_R \cos(2\pi f_e t + 2\pi f_b t + 2\pi/3)] \cos(2\pi f_e t + 2\pi/3)]$$

$$i_q = \frac{2}{3} [[A \cos(2\pi f_e t) + A_L \cos(2\pi f_e t - 2\pi f_b t) + A_R \cos(2\pi f_e t + 2\pi f_b t)] \sin(2\pi f_e t) + [A \cos(2\pi f_e t - 2\pi/3) + A_L \cos(2\pi f_e t - 2\pi f_b t - 2\pi/3) + A_R \cos(2\pi f_e t + 2\pi f_b t - 2\pi/3)] \sin(2\pi f_e t - 2\pi/3) + [A \cos(2\pi f_e t + 2\pi/3) + A_L \cos(2\pi f_e t - 2\pi f_b t + 2\pi/3) + A_R \cos(2\pi f_e t + 2\pi f_b t + 2\pi/3)] \sin(2\pi f_e t + 2\pi/3)]$$

From the multiplication identities of sines and cosines

$$\cos(\alpha) \cos(\beta) = \frac{1}{2} [\cos(\alpha + \beta) + \cos(\alpha - \beta)] \quad (4.17)$$

$$\cos(\alpha) \sin(\beta) = \frac{1}{2} [\sin(\alpha + \beta) - \sin(\alpha - \beta)] \quad (4.18)$$

expressions become

$$\begin{aligned} i_d = & \frac{2}{3} \frac{1}{2} (A[\cos(4\pi f_e t) + \cos(0)] + A_L[\cos(4\pi f_e t - 2\pi f_b t) + \cos(-2\pi f_b t)] + A_R[\cos(4\pi f_e t \\ & + 2\pi f_b t) + \cos(2\pi f_b t)] \\ & + A[\cos(4\pi f_e t - 4\pi/3) + \cos(0)] + A_L[\cos(4\pi f_e t - 4\pi/3 - 2\pi f_b t) + \cos(-2\pi f_b t)] + A_R[\cos(4\pi f_e t - \\ & 4\pi/3 + 2\pi f_b t) + \cos(2\pi f_b t)] \\ & + A[\cos(4\pi f_e t + 4\pi/3) + \cos(0)] + A_L[\cos(4\pi f_e t + 4\pi/3 - 2\pi f_b t) + \cos(-2\pi f_b t)] + A_R[\cos(4\pi f_e t \\ & + 4\pi/3 + 2\pi f_b t) + \cos(2\pi f_b t)]) \\ i_q = & \frac{2}{3} \frac{1}{2} (A[\sin(4\pi f_e t) - \sin(0)] + A_L[\sin(4\pi f_e t - 2\pi f_b t) - \sin(-2\pi f_b t)] + A_R[\sin(4\pi f_e t + 2\pi f_b t) - \\ & \sin(2\pi f_b t)] \\ & + A[\sin(4\pi f_e t - 4\pi/3) - \sin(0)] + A_L[\sin(4\pi f_e t - 4\pi/3 - 2\pi f_b t) - \sin(-2\pi f_b t)] + A_R[\sin(4\pi f_e t - \\ & 4\pi/3 + 2\pi f_b t) - \sin(2\pi f_b t)] \\ & + A[\sin(4\pi f_e t + 4\pi/3) - \sin(0)] + A_L[\sin(4\pi f_e t + 4\pi/3 - 2\pi f_b t) - \\ & \sin(2\pi f_b t)] + A_R[\sin(4\pi f_e t + 4\pi/3 + 2\pi f_b t) - \sin(2\pi f_b t)]) \end{aligned}$$

We know that, the sum of sines or cosines with equal amplitude and frequency displaced by 120° in phase is zero. By algebraic substitutions we get the simplified expression below

$$i_d = A_L \cos (2\pi f_b t) + A_R \cos (2\pi f_b t) \quad (4.19)$$

$$i_q = A_L \sin (2\pi f_b t) - A_R \sin (2\pi f_b t) \quad (4.20)$$

As A_L and A_R are equal to each other, i_q naturally becomes zero due to the equation (4.20). This brings out the reason of i_d to be chosen for signal pre-processing as current component.

Also expressions (4.19) and (4.20) state that, supply frequency is removed and only faulty rotor bar frequency is contained in the transformed equations, which leads us the way of analyzing the stator currents without using any notch filter.

5. ASSESSING OF THE ALGORITHM AND TESTING WITH REAL DATA

Matlab simulations are used to validate algorithm for the proposed method. After verifying the algorithm with simulated data, tests are carried out for both healthy and faulty (rotor with two broken bars) cases. Three phase currents are captured at 32 points per power system cycle for 256 cycles using the waveform capture capability of SquareD CM4000 Circuit Monitor. Then, the data is uploaded to a PC via the serial communication port and analyzed with the code written in matlab software.

The captured data has a decomposable bandwidth of 960 Hz since the sampling is done 32 points per power system cycle (60 Hz). The signal bandwidth is halved at each level and decomposing the signal by seven levels would achieve a 7.5 Hz bandwidth for each node.

5.1 TEST SETUP

The test system consists of a squirrel cage induction motor, a hysteresis dynamometer, Magtrol model HD-805, as the load, and a SquareD CM4000 Circuit Monitor for capturing motor current data. The test setup is depicted in figure 5.1.



Figure 5.1: Test setup for induction motor with a single broken rotor bar

The current data is captured using the waveform capture capability of a SquareD CM4000 Circuit Monitor. The Circuit Monitor has an onboard memory chip that provides storage for the captured data. Then, the data is uploaded to a PC via the serial communication port.

The sampled current signal contains the power system fundamental and other harmonic components. The broken rotor bar induced current spectrum components are significantly smaller than the power system harmonics in magnitude, therefore, some preprocessing of the signal is required to suppress the power system fundamental before the current signal is analyzed via wavelet packet analysis. The fundamental harmonic is eliminated by Park's transformation to minimize the error due to its leakage.

After transformation, the data is decomposed into equally spaced wavelet packets by using all-pass implementation of elliptic IIR half-band filter. Typically, 7.5 Hz wavelet packets would provide sufficient resolution for detecting broken rotor bar fault frequencies.

If the baseline of the wavelet packet coefficients is defined as the mean of these coefficients, non-zero baseline information may appear in a detail sub-band when the signal is contaminated by power system harmonic interference (Xu, 2005). The nonzero baseline stems from the contribution of harmonic interference only when special constraints among the interference between base frequency, sampling rate, and wavelet packet decomposition level is met. The baseline shifting is used to remove the effects of power system harmonics other than the fundamental.

5.2 TEST PROCEDURE

The basic steps of the algorithm are displayed in Figure 6.1. First baseline data for the motor is collected with a healthy set of bearings. The motor current data is then captured at user determined time intervals to check the status of bearings. The stator current data is notch filtered to suppress both the power system harmonics and rotor eccentricity frequency components. Then, the signal is decomposed into 7.5 Hz frequency bands using the fast wavelet packet algorithm. The all-pass implementation of elliptic half-band filters is used in the fast wavelet packet filter algorithm. The resulting wavelet packet coefficients are used to calculate the rms values for defect frequency bands. Finally, rms values for defect frequency bands are compared to baseline data to detect bearing faults and identify the type of the fault.

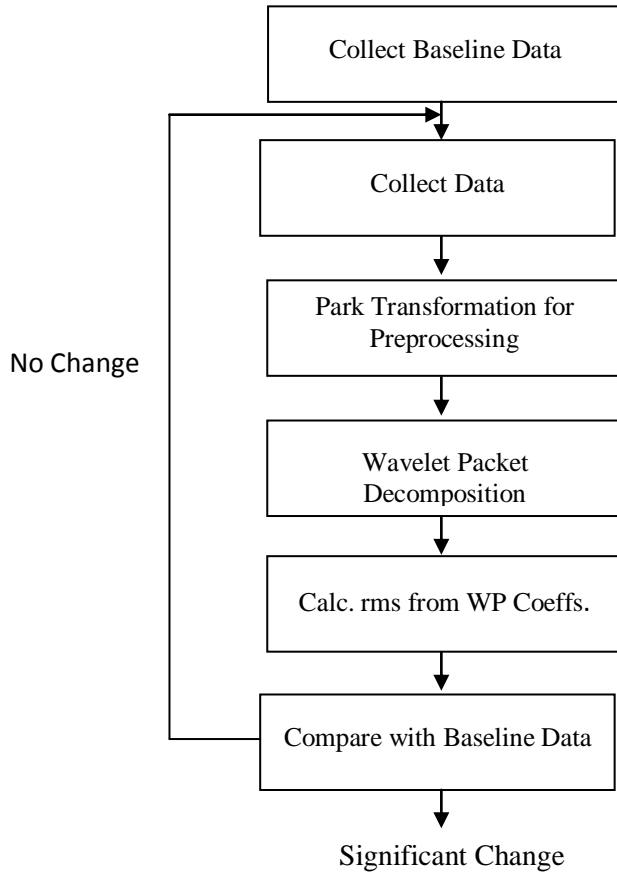


Figure 5.2: Flow chart Diagram

5.3 TESTING OF THE ALGORITHM USING SIMULATED DATA

In this section, the effectiveness of the proposed algorithm is tested with simulated data. Before the proposed algorithm is tested with both simulated and real data, the real data for a motor with both healthy rotor bars and two broken bars are analyzed with Fourier transform. The results are shown in figure 5.3.

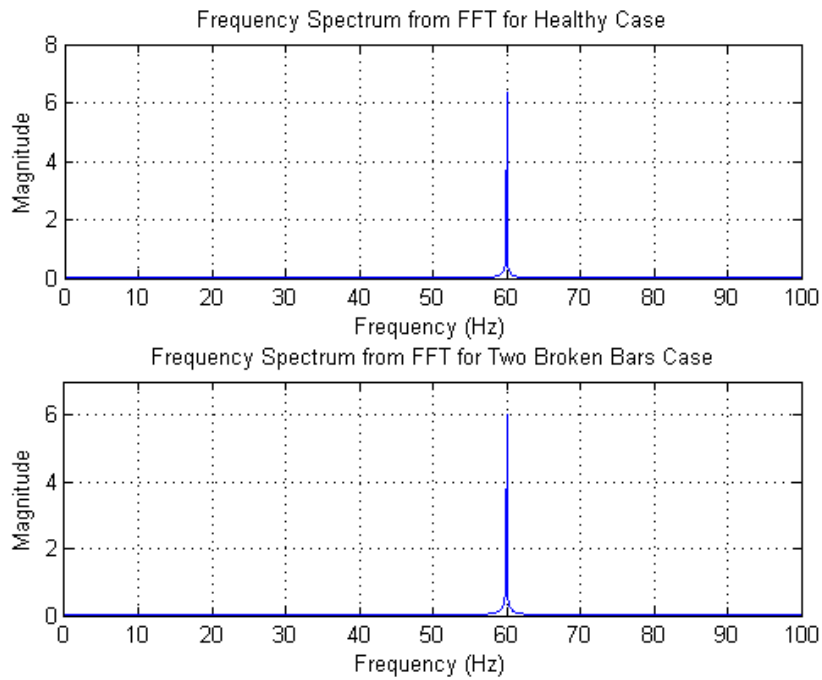


Figure 5.3: Both healthy rotor bars and two broken bars with Fourier transform

Here the fundamental component is so high compared to broken rotor bar frequencies that healthy case cannot be discriminated from the faulty case. It is obvious from the figure that preprocessing of current signal is required to suppress the fundamental component. The preprocessing means additional computational burden. In the proposed method, the fundamental is suppressed by Park's transformation and the fault signal is demodulated making it easier to identify at a minimal computational cost.

The test data includes 6 Hz fault signal modulated to the line frequency of 60 Hz. The magnitude of the fault frequency component is designed to be 10 % of the fundamental component. The matlab code for generating the faulty data is given in the Appendix A. The simulated data has a length of 8192 points at 32 point per cycle.

One of the phase currents for the simulated data is depicted in figure 5.4. Here, only the first four cycles are plotted.

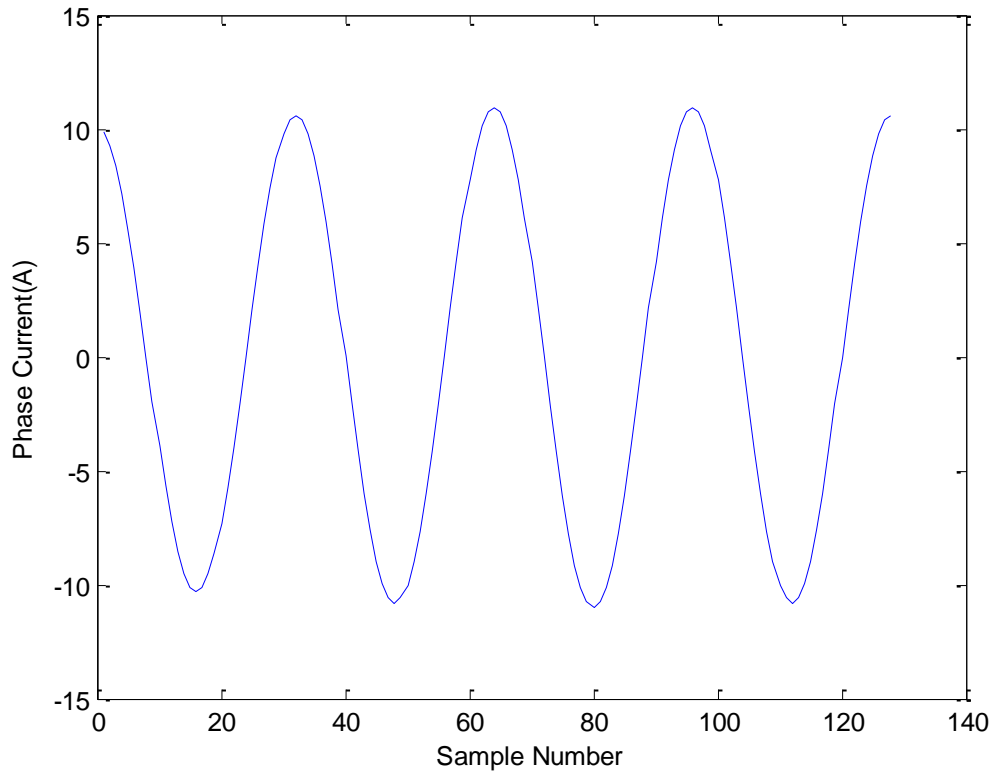


Figure 5.4: Simulated phase current

The simulated data is depicted into direct and quadrature components using Park's transformation. The direct current component is plotted in figure 5.5. The data length in this figure is 8192 sample points. It is obvious from the figure that there are 26 cycles in the observation period. Considering the fact that the simulated data had 256 cycles of the fundamental frequency (60 Hz) in 8192 sample points, the length of 26 cycles would correspond to the fault frequency very close to 6 Hz.

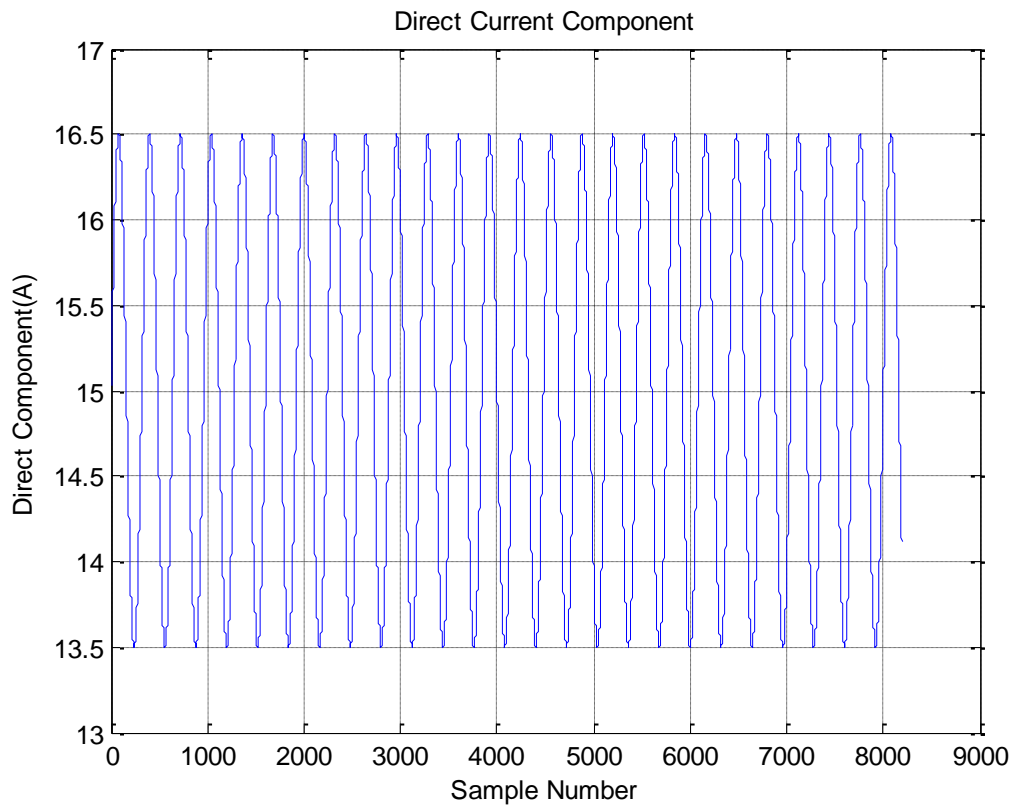


Figure 5.5: Direct current component from Park's transformation

The direct current component data is then decomposed into wavelet packets using the fast wavelet packet decomposition algorithm. Here, packets are designed such that each packet has 7.5 Hz bandwidth. Since the fault frequency is around 6 Hz, only the node that covers 0-7.5 Hz band must be analyzed. The wavelet packet coefficients for the fault associated node is plotted in figure 5.6. The coefficients plotted in this figure indicate a periodic waveform.

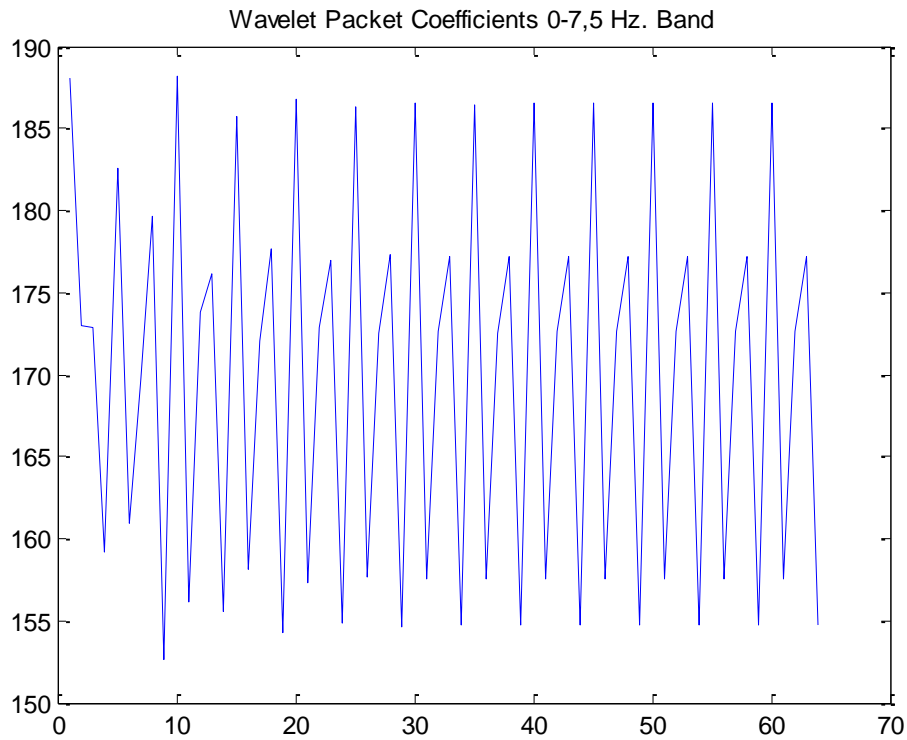


Figure 5.6: Wavelet Packet Coefficients 0-7.5 Hz. Band

In order to verify that the energy associated with this band is due to 6 Hz fault component, the fast Fourier transform may be utilized. The result of the frequency analysis is shown in figure 5.7. Here, it is obvious from the figure that only frequency component in this frequency band is 6 Hz.

After verifying that the algorithms works well with simulated data, the motor current data captured with SquareD Circuit Monitor is analyzed.

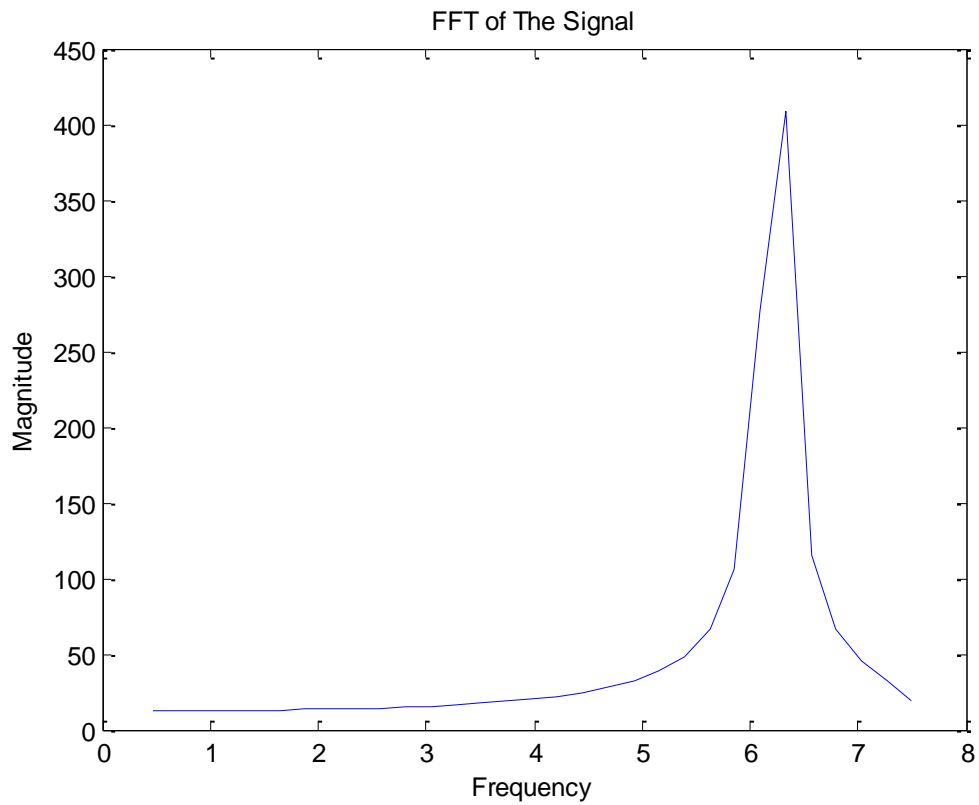


Figure 5.7: FFT of the direct component

5.4 TESTING WITH HEALTHY MOTOR DATA

In the second section, the proposed method is tested with real motor data. In the first part, a motor with no broken bars is tested. The motor is ran at 1740 rpm and full load. The dynamometer is used as the load. One of the phase currents for the captured data is depicted in figure 5.8. Here, only the first four cycles are plotted.

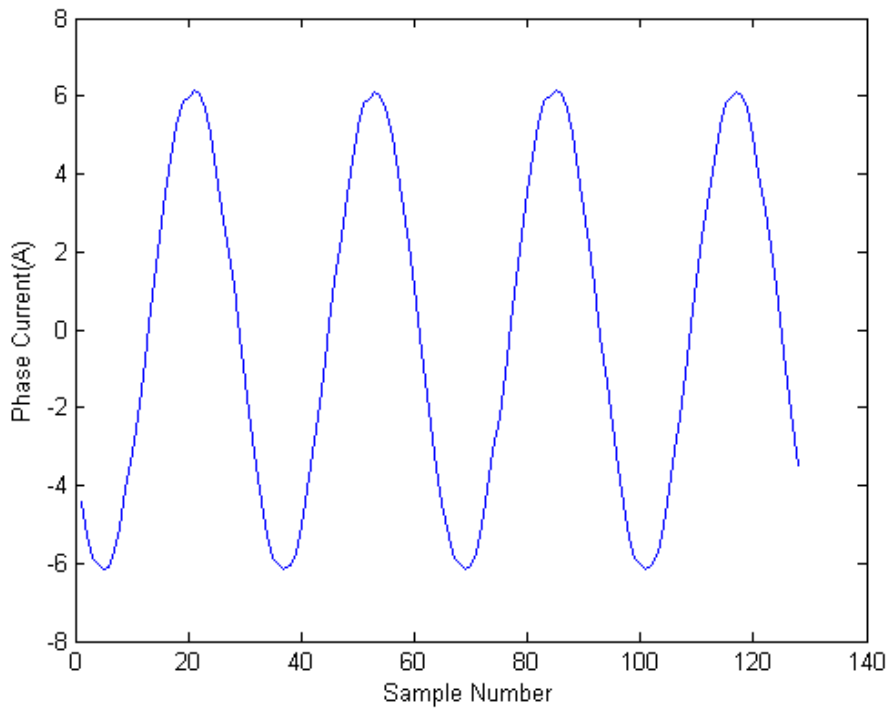


Figure 5.8: Healthy case phase current

The captured data is decomposed into direct and quadrature components using Park's transformation. The direct current component is plotted in figure 5.9. The data length in this figure is 8192 sample points.

The direct current component data is then decomposed into wavelet packets using the fast wavelet packet decomposition algorithm. Here, packets are designed such that each packet has 7.5 Hz bandwidth. Since the fault frequency is around 4 Hz, only the node that covers 0-7.5 Hz band must be analyzed. The wavelet packet coefficients for the fault associated node is plotted in figure 5.10. The coefficients plotted in this figure do not indicate a periodic waveform. The energy level for this node is calculated to be 0.66 Amperes. This value will be compared to the faulty case in the next section.

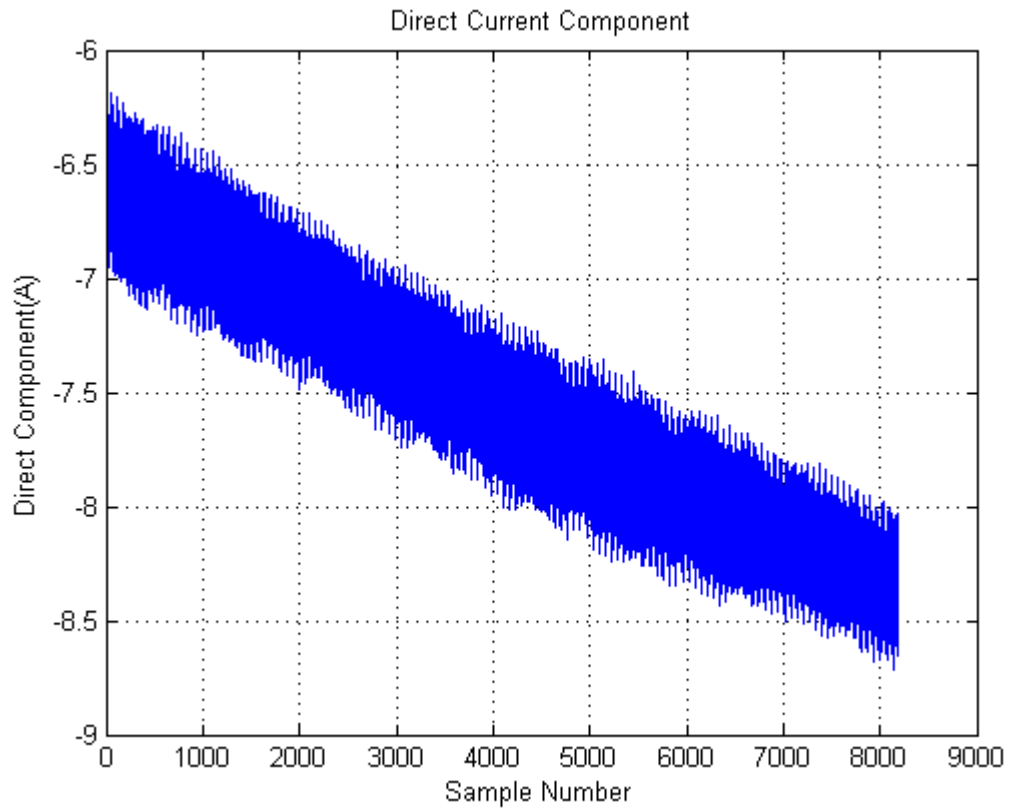


Figure 5.9: Direct current component

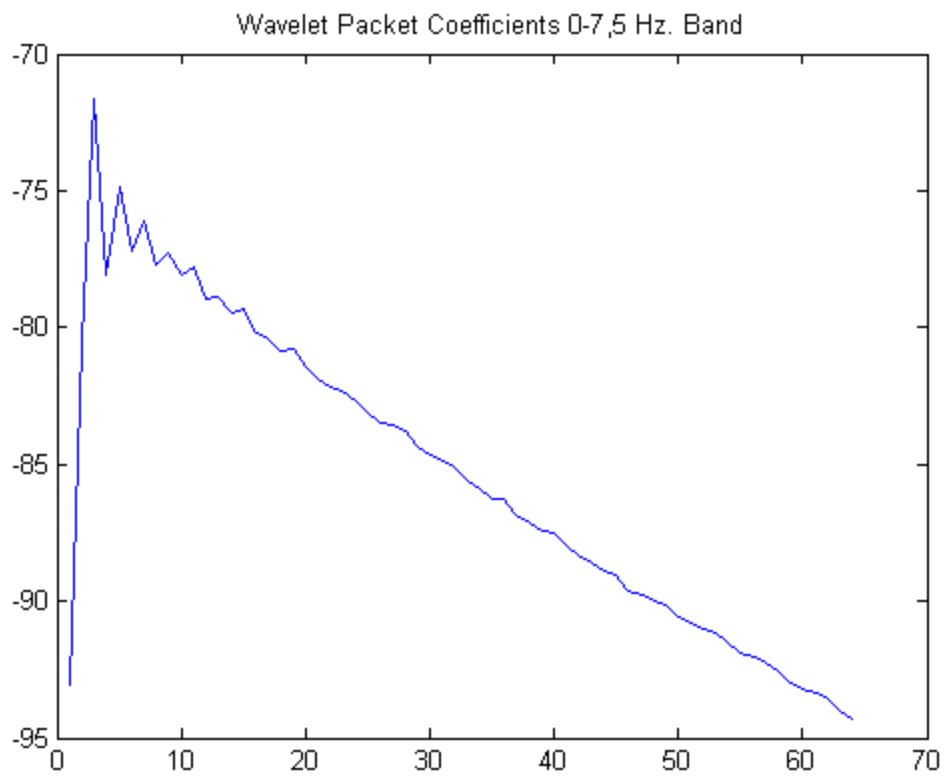


Figure 5.10: Wavelet Packet Coefficients 0-7.5 Hz. Band

In order to verify that the energy associated with this band is due to 4 Hz fault component, the fast Fourier transform may be utilized. The result of the frequency analysis is shown in figure 5.11. Here, it is obvious from the figure that broken rotor bar frequency is not very pronounced here.

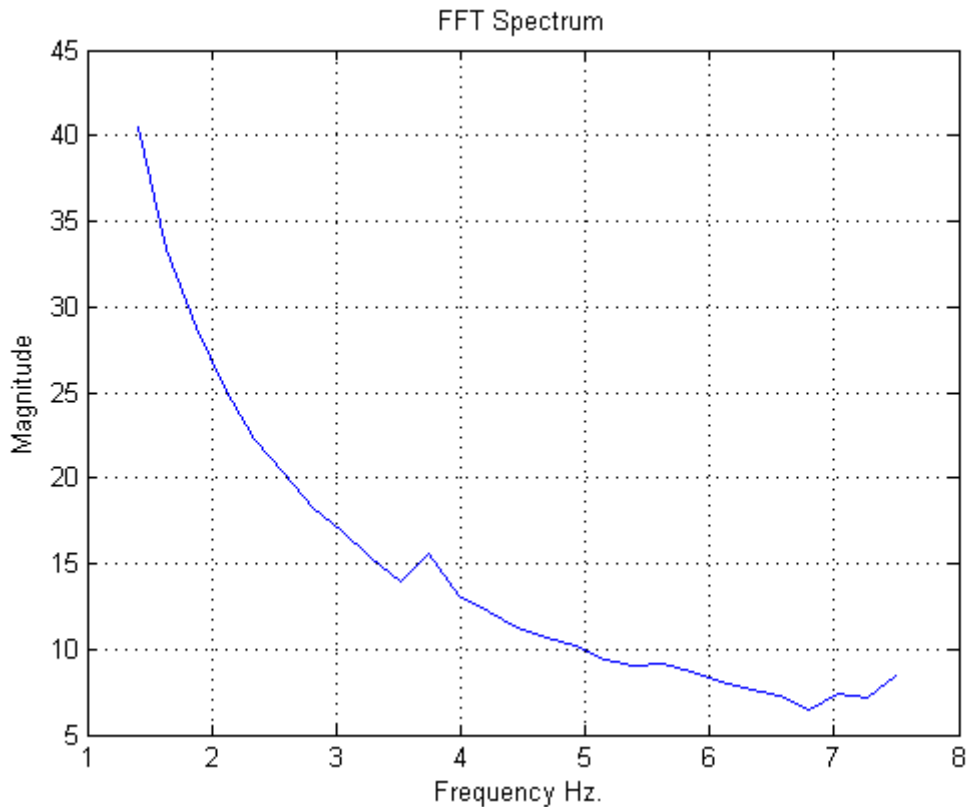


Figure 5.11: FFT of the direct component

5.5 TESTING WITH FAULTY MOTOR DATA

In the second part, a motor with two broken bars is tested. The motor is ran at 1740 rpm and full load. The dynamometer is used as the load. One of the phase currents for the captured data is depicted in figure 5.12. Here, only the first four cycles are plotted.

The captured data is decomposed into direct and quadrature components using Park's transformation. The direct current component is plotted in figure 5.13. The data length in this figure is 8192 sample points.

The direct current component data is then decomposed into wavelet packets using the fast wavelet packet decomposition algorithm. Here, packets are designed such that each packet has 7.5 Hz bandwidth. Since the fault frequency is around 4 Hz, only the node that covers 0-7.5 Hz band must be analyzed. The wavelet packet coefficients for the fault associated node is plotted in figure 5.14. The coefficients plotted in this figure indicate a periodic waveform. The energy level for this node is calculated to be 1.89 Amperes. This value is clearly much higher (about three times) than the healthy case analyzed in the previous section.

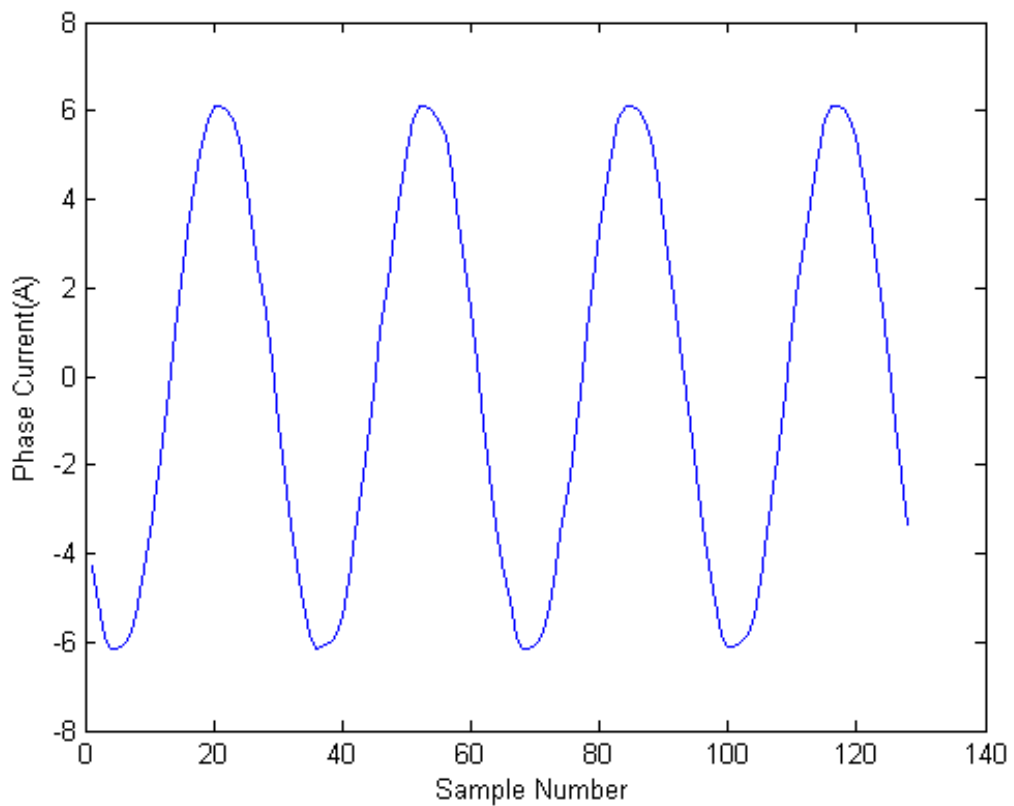


Figure 5.12: Faulty case phase current

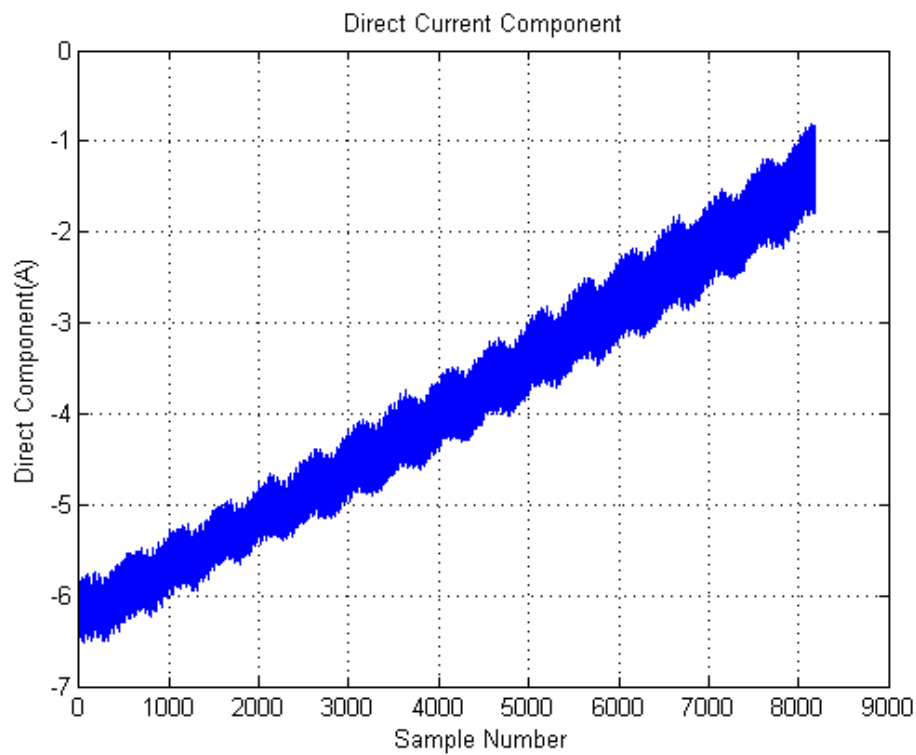


Figure 5.13: Direct current component

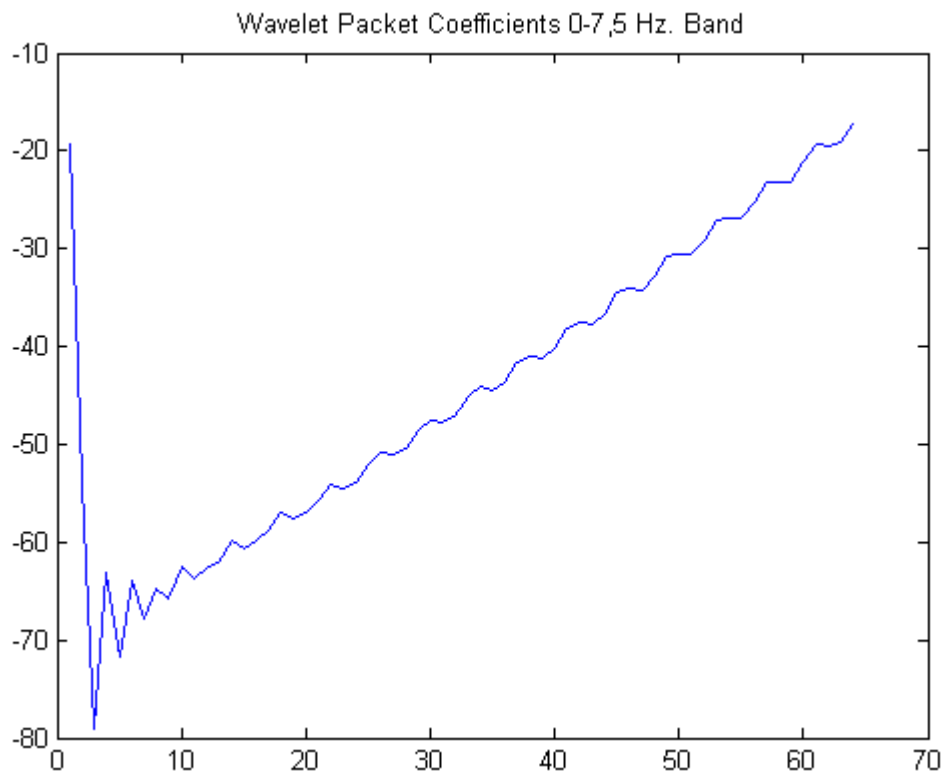


Figure 5.14: Wavelet Packet Coefficients 0-7.5 Hz. Band

In order to verify that the energy associated with this band is due to 4 Hz fault component, the fast Fourier transform may be utilized. The result of the frequency analysis is shown in figure 5.15. Here, it is obvious from the figure that broken rotor bar frequency is very pronounced here.

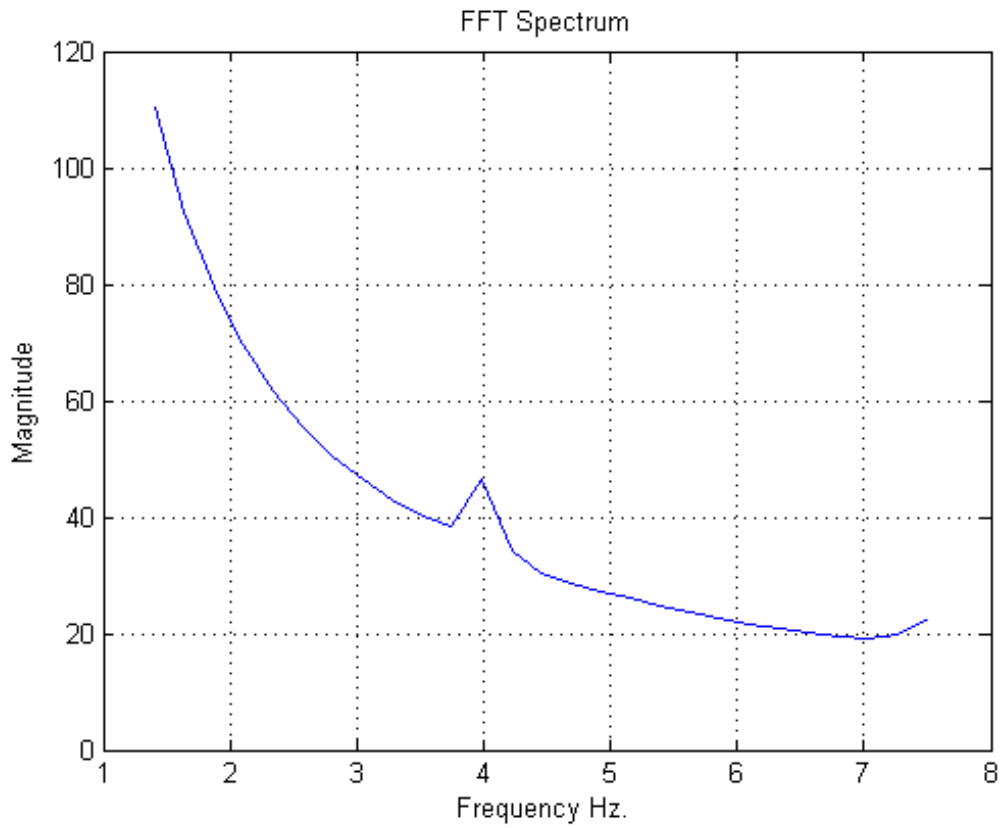


Figure 5.15: FFT of the direct component

6. CONCLUSION AND FUTURE WORK

The broken rotor bar frequency components are very small compared to the power system fundamental frequency component making broken rotor bar detection very difficult at rated speed operation. Usually some preprocessing is required to suppress the fundamental frequency resulting in further computational burden. It is also very difficult to suppress the fundamental frequency component without affecting the magnitudes of broken rotor bar related frequency components since they are very close to the fundamental. In this work, the use of Park's transformation in fundamental frequency suppression for wavelet packet based broken rotor bar detection is proposed. In the proposed method, the fundamental frequency component is suppressed in direct current component obtained from Park's transformation applied to three phase currents. This is also shown through mathematical derivations in section 4.3.

Then, the direct current component is decomposed into equally spaced frequency bands by using all-pass implementation of elliptic IIR half-band filter. Next, energy level of each frequency band is calculated by determining rms values from WPCs of associated frequency bands. The changes in the energy levels of frequency bands in which broken rotor bar related current frequencies lie are monitored to detect motor fault condition.

In order to verify that the increase in the energy levels of fault associated frequency bands are indeed due to the broken rotor bars, spectral post processing was applied. Both simulated and real data showed that the proposed approach is effective in detecting broken rotor bars.

The performance of different filters in wavelet packet decomposition may be explored for future work. Also, different motor fault conditions such as bearing faults may be included in the future study.

REFERENCES

Books

Fitzgerald, A.E., Kingsley, C. and Umans, S.D.,2002. *Electric machinery*. McGraw-Hill

Krause, P. C.; Wasynczuk, Oleg; Sudhoff, Scott D., 2002. *Analysis of Electric Machinery and Drive Systems*.Wiley-IEEE Press.

Smith, S. W., 1997. *The Scientist and Engineer's Guide to Digital Signal Processing*. California Technical Publishing

Periodical

Publications

Arslan, H., Orhan, S., Aktürk, N., 2003. *Bilyeli Rulman Hasarlarının Neden Olduğu Titreşimlerin Modellenmesi*. Gazi Üniv. Müh. Mim. Fak. Der Cilt 18, No 4, 123-146.

Bellini, A. Filippetti, F. Franceschini, G. Tassoni, C. Kliman, G.B., "*Quantitative evaluation of induction motor broken bars by means of electrical signature analysis*," IEEE Transactions on Industry Applications, vol. 37, pp. 1248-1255, 2001.

Benbouzid, M.E.H. Nejjari, H. Beguenane, R. Vieira, M., "*Induction motor asymmetrical faults detection using advanced signal processing techniques*," IEEE Trans. on Energy Conversion, vol. 14, no. 2, pp. 147–152, 1999.

Bonaldi, E.L.; de Oliveira, L.Ede.L.; da Silva, L.E.B.; Torres, G.L.; *Removing the fundamental component in MCSA using the synchronous reference frame approach*. 2003 IEEE International Symposium on Industrial Electronics. Issue Date: 9-11 June 2003 On page(s): 913 - 918 vol. 2

Cusido J., Rosero J. A., Ortega J. A., Garcia A., Romeral L., *Induction motor fault detection by using wavelet decomposition on dq0 components*, IEEE ISIE 2006, Montreal, Quebec, Canada, 2006, pp. 2406–2411.

Eren, L.; Devaney, M.J. *Motor bearing damage detection via wavelet analysis of the starting current transient*, Proceedings of the 18th IEEE Instrumentation and Measurement Technology Conference, 2001, Vol. 3, pp. 1797 –1800.

Eren,L., Çekiç Y., Devaney M.J., *Broken Rotor Bar Detection via Wavelet Packet Decomposition of Motor Current* International Review of Electrical Engineering, Vol.4, N.5 September-October 2009

Graps, A., 1995. *An Introduction to Wavelets*. IEEE Computational Sciences and Engineering, Volume 2, Number 2, 50-61.

Kliman G.B., Premerlani W.J., Yazici B., Koegl R.A., and Mazereeuw J., *Sensorless online motor diagnostics*, IEEE Comput.Appl. Power, vol. 10, no.2, pp. 39–43, 1997.

Kliman, G.B. Koegl, R.A. Stein, J. Endicott, R.D. Madden, M.W., *Noninvasive detection of broken rotor bars in operating induction motors*, *IEEE Trans. Energy Conversion*, vol. 3, no. 4, pp. 873-879, Dec. 1988.

Kryter R.C. and Haynes H.D., *Condition monitoring of machinery using motor current signature analysis*, *Sound and Vibration*, pp. 14-21, Sept. 1989.

L. Xu, *Cancellation of harmonic interference by baseline shifting of wavelet packet decomposition coefficients*, *IEEE Transactions on Signal Processing*, vol. 53, no 1, pp. 222-30, Jan. 2005.

M. E. H. Benbouzid., "A review of induction motors signature analysis as a medium for faults detection," *IEEE Transactions on Industrial Electronics*, vol. 47, pp. 984-993, 2000.

Mehla N., Dahiya R. *Motor Current Signature Analysis and its Applications in Induction Motor Fault Diagnosis*, *international journal of systems applications, engineering & development* Issue 1, Volume 1, 2007

Nandi, S. Toliyat, H.A. Xiaodong Li, "Condition Monitoring and Fault Diagnosis of Electrical Motors - A Review," *IEEE Transactions on Energy Conversion*, vol. 20, pp. 719-729, 2005.

P.Pilly and Z. Xu, *Motor Current Signature Analysis* Clarkson University ECE Department

Rioul, O., Vetterli, M., 1991. *Wavelets and Signal Processing*. *Signal Processing Magazine IEEE*, Volume: 8, Issue: 4, 14–38.

Şeker S., Ayaz E., *Feature Extraction Related to Bearing Damage in Electric Motors by Wavelet Analysis*, *Journal of the Franklin Institute*, Vol.340, Issue 2, March 2003, pp. 125-134.

Thomson, W.T.; Fenger, M., "Current signature analysis to detect induction motor faults," *IEEE Ind. Appl. Magn.*, vol. 7, no. 4, pp. 26–34, Aug. 2001.

Other Publications

Gwyddion user guide, <http://gwyddion.net/documentation/user-guide-en/index.html>

POLIKAR R., *The Wavelet Tutorial*

Misiti M., Misiti Y., Oppenheim G., Poggi, J.M., *Wavelet Toolbox For Use with MATLAB*

APPENDIX

A.1 WAVELET PACKET ALGORITHM

```
b2=[0.519974 1];
a2=[1 0.519974];
b1=[0.145612596 1.016102 1];
a1=[1 1.016102 0.145612596 ];
t=[1:1:8192];

fid = fopen('healthy1.txt','r');
[D,COUNT] = fscanf(fid,'%f');
fclose(fid);
Ic=D([7:7:COUNT]);
Ib=D([6:7:COUNT]);
Ia=-(Ib+Ic);

figure(1);
plot(t(1:128),downsample(Ia(1:512),4));
xlabel('Sample Number');
ylabel('Phase Current(A)');

for i=1:128*256
Iq(i)=-Ia(i)*sin(2*pi*i/128)-Ib(i)*sin(2*pi*i/128-pi/1.5)-Ic(i)*sin(2*pi*i/128+pi/1.5);
Id(i)=Ia(i)*cos(2*pi*i/128)+Ib(i)*cos(2*pi*i/128-pi/1.5)+Ic(i)*cos(2*pi*i/128+pi/1.5);
I0(i)=Ia(i)+Ib(i)+Ic(i);
end

figure(2);
plot(downsample(Id,4));
title('Direct Current Component');
xlabel('Sample Number');
ylabel('Direct Component(A)');
```

```

grid on;
%axis([0 8192 13,5 16,5]);
beta=downsample(Id,4);

for i=1:7
    for k=1:2^(i-1)
        ind=2*(k-1);
        [y1,y2]=downsample2(beta((k-1)*length(beta)/2^(i-1)+1:(k)*length(beta)/2^(i-1)));
        [y12]=filtre3(b1,a1,y1);
        [y22]=filtre2(b2,a2,y2);

        betax=(y12+y22)/sqrt(2);
        alfax=(y12-y22)/sqrt(2);
        clear y12;
        clear y22;
        beta(ind*length(beta)/2^i+1:(ind+1)*length(beta)/2^i)=betax;
        beta((ind+1)*length(beta)/2^i+1:(ind+2)*length(beta)/2^i)=alfax;
    end
end
mag7=abs(fft(beta(1:64)));

figure(3);
plot(beta(1:64));
title('Wavelet Packet Coefficients 0-7,5 Hz. Band');

Tx=[7.5/32:7.5/32:7.5];
figure(4);
plot(Tx(6:32),mag7(6:32));
title('FFT Spectrum');
xlabel('Frequency Hz. ');
ylabel('Magnitude');

```

A.2 SIMULATION ALGORITHM

```
for i=1:32*256
Va(i)=10*cos(2*pi*i/32);
Vb(i)=10*cos(2*pi*i/32-pi/1.5);
Vc(i)=10*cos(2*pi*i/32+pi/1.5);
end
modsin =sin(0.1*pi*t/32);
xt=1+0.1*modsin;
Va=Va.*xt;
Vb=Vb.*xt;
Vc=Vc.*xt;
for i=1:32*256
Vq(i)=-Va(i)*sin(2*pi*i/32)-Vb(i)*sin(2*pi*i/32-pi/1.5)-Vc(i)*sin(2*pi*i/32+pi/1.5);
Vd(i)=Va(i)*cos(2*pi*i/32)+Vb(i)*cos(2*pi*i/32-pi/1.5)+Vc(i)*cos(2*pi*i/32+pi/1.5);
V0(i)=Va(i)+Vb(i)+Vc(i);
end
beta=Vd;
for i=1:7
for k=1:2^(i-1)
ind=2*(k-1);
[y1,y2]=downsample2(beta((k-1)*length(beta)/2^(i-1)+1:(k)*length(beta)/2^(i-1)));
[y12]=filtre3(b1,a1,y1);
[y22]=filtre2(b2,a2,y2);
betax=(y12+y22)/sqrt(2);
alfax=(y12-y22)/sqrt(2);
clear y12;
clear y22;
beta(ind*length(beta)/2^(i)+1:(ind+1)*length(beta)/2^(i))=betax;
beta((ind+1)*length(beta)/2^(i)+1:(ind+2)*length(beta)/2^(i))=alfax;
end
end
mag7=abs(fft(beta(1:64)));
plot(mag7(3:64));
```

A.3 FILTERING FUNCTIONS

```
function [yw2]=filtre3(b,a,x)
xx=[x x];

for i=1:length(b)-1
    yw(i)=0;
end
for i=length(b):length(xx)
    yw(i)=b(1)*xx(i)+b(2)*xx(i-1)+b(3)*xx(i-2)-a(2)*yw(i-1)-a(3)*yw(i-2);
end

yw2=yw(length(xx)/2+1:length(xx));
```

```
function [yw2]=filtre2(b,a,x)
xx=[x x];

for i=1:length(b)-1
    yw(i)=0;
end
for i=length(b):length(xx)
    yw(i)=b(1)*xx(i)+b(2)*xx(i-1)-a(2)*yw(i-1);
end

yw2=yw(length(xx)/2+1:length(xx));
```

```
function xx = myg(L)
for i=0:2^L-1
    x=0;
    y=mgraycode(i,L);
    for j=L:-1:1
        x=x+y(L-j+1)*2^(j-1);
    end
    xx(i+1)=x;
end
```

CURRICULUM VITAE

Name and Surname : Ferzan GÜRAN

Permanent Address : Mustafamazharbey Cad. Çamtepe Sok. Huzur Apt. 15/16
Kadıköy/İstanbul

Birth Place and Year : Üsküdar, 1976

Languages : Turkish (native) - English

High School : Kadıköy Anadolu Lisesi 1990 - 1993

Undergraduate Degree : Yıldız Teknik Üniversitesi 1994 - 2008

Graduate Degree : Bahçeşehir Üniversitesi 2009 - 2011

Name of Institute : Institute of Science

Name of Program : Electrical and Electronics Engineering

Work Experience : Çekmeköy Municipality 2009 - Ongoing